



**HAL**  
open science

## A minimal predictive model for better formulations of solvent phases with low viscosity

Maximilian Pleines, Maximilian Hahn, Jean Duhamet, Thomas Zemb

► **To cite this version:**

Maximilian Pleines, Maximilian Hahn, Jean Duhamet, Thomas Zemb. A minimal predictive model for better formulations of solvent phases with low viscosity. EPJ N - Nuclear Sciences & Technologies, 2020, 6, pp.3. 10.1051/epjn/2019055 . cea-02458352

**HAL Id: cea-02458352**

**<https://cea.hal.science/cea-02458352v1>**

Submitted on 28 Jan 2020

**HAL** is a multi-disciplinary open access archive for the deposit and dissemination of scientific research documents, whether they are published or not. The documents may come from teaching and research institutions in France or abroad, or from public or private research centers.

L'archive ouverte pluridisciplinaire **HAL**, est destinée au dépôt et à la diffusion de documents scientifiques de niveau recherche, publiés ou non, émanant des établissements d'enseignement et de recherche français ou étrangers, des laboratoires publics ou privés.

# A minimal predictive model for better formulations of solvent phases with low viscosity

Maximilian Pleines<sup>1,2</sup>, Maximilian Hahn<sup>2,3</sup>, Jean Duhamet<sup>4,\*</sup>, and Thomas Zemb<sup>1</sup>

<sup>1</sup> Institute for Separation Chemistry, ICSM, CEA, CNRS, ENSCM, Univ. Montpellier, Marcoule, France

<sup>2</sup> Department of Physical Chemistry, University of Regensburg, 93051 Regensburg, Germany

<sup>3</sup> COSMOlogic GmbH & Co. KG, 51379 Leverkusen, Germany

<sup>4</sup> CEA, DEN, DMRC, Univ. Montpellier, Marcoule, France

Received: 20 August 2019 / Received in final form: 10 October 2019 / Accepted: 13 November 2019

**Abstract.** The viscosity increase of the organic phase when liquid–liquid extraction processes are intensified causes difficulties for hydrometallurgical processes on industrial scale. In this work, we have analyzed this problem for the example of *N,N*-dialkylamides in the presence of uranyl nitrate experimentally. Furthermore, we present a minimal model at nanoscale that allows rationalizing the experimental phenomena by connecting the molecular, mesoscopic and macroscopic scale and that allows predicting qualitative trends in viscosity. This model opens broad possibilities in optimizing constraints and is a further step towards knowledge-based formulation of extracting microemulsions formed by microstructures with low connectivity, even at high load with heavy metals.

## 1 Introduction

Liquid–liquid extraction is the central technology in metal recycling [1,2]. An important application is the recovery of major actinides – Uranium and Plutonium – in the framework of minimization of highly radioactive waste by use of Mixed Oxide Fuel (MOX) and the required closing of the nuclear fuel cycle by using fast neutrons in the future [3].

Designing efficient metal recovery processes based on solvent extraction is not a straightforward task due to the low solubility of inorganic ions in oils. In an optimized formulation, oil-soluble complexing molecules are required to (a) complex these ions selectively and (b) to solubilize the resulting complexes in the organic phase. These so-called extractants are surface-active molecules that are composed of a polar complexing group, a Lewis base, and an apolar moiety that increases the solubility of the molecules in the organic diluent [4]. Since the pioneering proposition of the existence of water-poor microemulsions as w/o micelles by Osseo-Assare in 1991, solvent extraction in hydrometallurgy has been recognized as based on one phase transfer involving self-assembly and micellization in conjunction with supramolecular complexation by “extractants” in first and second coordination spheres [5]. This so-called “ieanic” approach has been recently backed up by

combined small angle scattering and molecular dynamic simulations [6]. Compared to classical microemulsions, the gain in free energy arising from formation of aggregates is lower. Therefore, these microemulsions belong to the class driven by “weak aggregation” [7].

Even if the processes using Tributyl phosphate (TBP) as selective extractant are known since world-war II, economic and technical reasons motivate the research for alternative extractants. One promising approach that is under development since several years is the use of *N,N*-dialkylamides which also have a high affinity towards Uranium and Plutonium and significant advantages over TBP [8–11]. The main disadvantage of *N,N*-dialkylamides is the viscosity of the organic phase which increases exponentially when processes are intensified by increasing uranyl and extractant concentration [12]. Emulsification and demulsification in industrial extraction devices is only efficient when the difference in viscosity between organic and aqueous phase is small [13,14]. The problem of viscosity in solvent extraction was already treated for ionic liquids [15] and vanadium extracting systems [16] in this journal.

The extraction and coordination of major actinides by *N,N*-dialkylamides has been intensively studied in the last decades [10,17–21]. Ferru and co-workers have been the first to investigate the aggregation behavior at molecular and supramolecular scale at elevated extractant concentration by combining molecular dynamics and X-ray scattering [6,22,23]. At elevated uranyl content that is

\* e-mail: [jean.duhamet@cea.fr](mailto:jean.duhamet@cea.fr)

representative for industrial extraction processes, they observed a strongly structured organic solution of  $N,N$ -dialkylamides diluted in heptane. The structure is formed by complexes of major stoichiometry  $UO_2(NO_3)_2L_2$  that are partly linked via bridging nitrates [6]. Consequently, long linear  $(-UO_2(NO_3)_2-)_n$  threads were found for 0.5 M extractant in the organic phase. These investigations have given a first insight into the structure evolution of  $N,N$ -dialkylamides with increasing uranyl concentration, but do not allow a generalization of the phenomenon.

Until now, the approaches to tackle the optimization of formulations at the extraction as well as stripping stages are based on experimental investigations along “*experimental design*” [24]. These long suite of experiments find by trial-and-error a compromise between selectivity and hydrodynamic properties such as viscosity and interfacial tension. To our best knowledge, there is no published explicit predictive model that proposes explanations of the viscosity increase by quantitative thermodynamic and nanostructural arguments.

In this work, we propose a first thermodynamic model that allows understanding the observed differences between certain extractants as well as the influence of diluent and solute concentration on the viscosity of the organic phase and the underlying microstructure.

## 2 Materials and methods

### 2.1 Materials

The dialkylamide extractants DEHBA ( $N,N$ -(2-ethylhexyl)butyramide), DEHiBA ( $N,N$ -(2-ethylhexyl)isobutyramide), DEHDMBA ( $N,N$ -(2-ethylhexyl)dimethylbutyramide) and MOEHA ( $N$ -methyl- $N$ -octyl-(2-ethyl)hexanamide) were synthesized by Pharmasynthese (Lisses, France) with a purity higher than 99%. Tributyl phosphate (purity >97%),  $n$ -octanol (>99%),  $n$ -dodecane (>99%) and *iso*-octane (>99%) were purchased from Sigma-Aldrich, Isane IP 175 from TOTAL Special Fluids. The chemical structure of the extractants is presented in Figure 1.

### 2.2 Sample preparation

Organic phases were prepared by diluting a certain extractant in a diluent to reach a definite molarity. After that, the solutions were contacted for 3 h with aqueous phases of equal volumes. The aqueous phase consisted of diluted uranyl nitrate in different concentrations at a constant acid molarity of 3 M nitric acid. The two phases were separated after centrifugation. In order to prepare an organic phase of a definite uranyl content, the concentration of uranyl in the aqueous phase was chosen so that the intended concentration of the organic phase is reached after contact of the two phases according to the known distribution coefficients. The uranyl content was determined volumetrically. This procedure includes first a quantitative reduction of uranium(VI) to uranium(IV) by a hydrochloric solution of Titan(III) chloride (Merck, 15%)

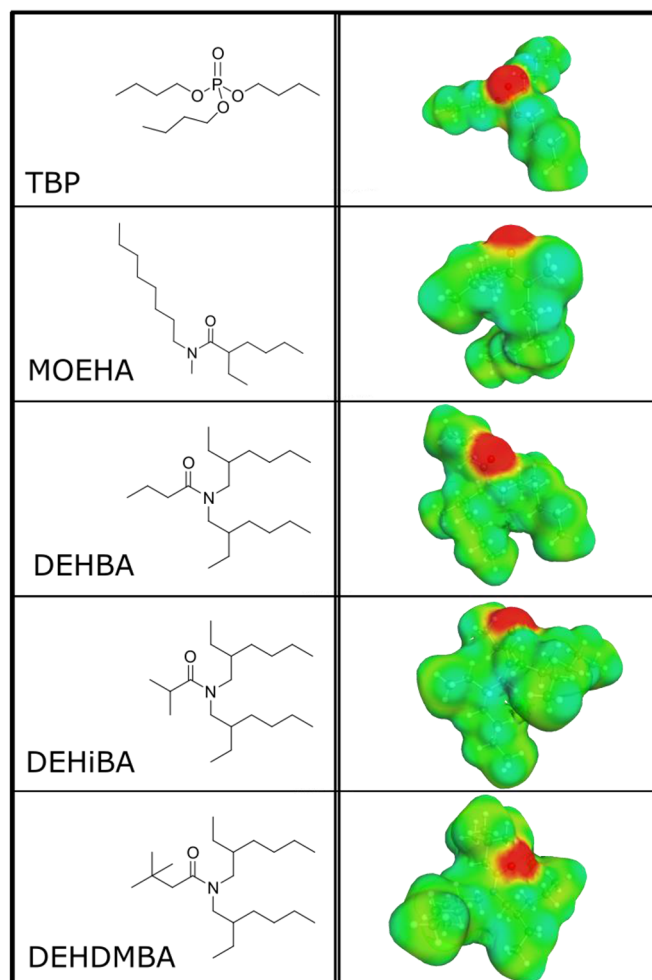


Fig. 1. Extractant structure and COSMO cavities.

and second a back-oxidation to hexavalent uranium by  $FeCl_3$  (27%, VWR). The amount of  $Fe^{2+}$ , which is related to the amount of  $U^{6+}$ , is determined by potentiometric titration with 0.1 N Titrimorm potassium dichromate solution (Volusol) [25,26].

### 2.3 Viscosity measurements

Viscosity measurements were carried out with an Anton Paar DSR 301 Rheometer under thermostatic control using a couette CC17 T200 SS geometry (diameter 16.666 mm; length 24.995 mm). The sample volume was 4 mL. The geometry of concentric cylinders was chosen because of security reasons and to minimize evaporation effects. Since all measured solutions behaved Newtonian, a certain shear rate (50 1/s) was chosen as representative value for the viscosity. It was intentionally forgone to extrapolate the curves to obtain the zero shear viscosity, since the data at low shear rates were noisy and the presence of a yield stress could not be excluded for each case. Shear viscosities were measured under thermostatic control from shear rates of 0.1–1000 1/s with 10 points per decade and a measurement duration of 6 s/point. Each measurement was carried out three times and the mean value was taken for plotting.

The standard deviation for these measurements was approximately 0.1–0.3 mPa s. Since this standard deviation is small for elevated viscosities, error bars are not shown for reason of better clarity. In the following text, the term “viscosity” is used equivalently for “shear viscosity”.

## 2.4 Scattering experiments

Small- and Wide-Angle X-ray Scattering (SAXS) experiments were carried out on a bench built by Xenocs using X-ray radiation from a molybdenum source ( $\lambda = 0.71 \text{ \AA}$ ) delivering a 1 mm large circular beam of energy 17.4 keV. The scattered beam was recorded by a large online scanner detector (MAR Research 345) which was located 750 mm from the sample stage. Off-center detection was used to cover a large  $q$  range simultaneously ( $0.2 \text{ nm}^{-1} < q < 30 \text{ nm}^{-1}$ ,  $q = [4\pi/\lambda]\sin(\theta/2)$ ). Collimation was applied using a 12:∞ multilayer Xenocs mirror (for Mo radiation) coupled to two sets of Forvis<sup>tm</sup> scatterless slits which provides a  $0.8 \text{ mm} \times 0.8 \text{ mm}$  X-ray beam at the sample position. A high-density polyethylene sample (from Goodfellow) was used as a calibration standard to obtain absolute intensities. Silver behenate in a sealed capillary was used as scattering vector calibration standard. Data were normalized taking into account the electronic background of the detector, transmission measurements as well as empty cell and fluorescence subtraction [6].

Small-angle neutron scattering (SANS) were performed at the French neutron facility Laboratoire Leon Brillouin (LLB) on the PAXY spectrometer using four configurations (sample-to-detector distance  $d = 1 \text{ m}$ , wavelength  $\lambda = 4 \text{ \AA}$ ,  $d = 6 \text{ m}$ ,  $\lambda = 3 \text{ \AA}$ ,  $d = 8.5 \text{ m}$ ,  $\lambda = 5 \text{ \AA}$ ,  $d = 15 \text{ m}$ ,  $\lambda = 6.7 \text{ \AA}$ ) to cover a  $q$ -range from 0.0019 to  $0.64 \text{ \AA}^{-1}$ . Measurements were performed in quartz Hellma cells of an optical path of 1 mm. At low  $q$ , the measurement time was set to 4 h in order to deliver sufficiently high statistics. Correction of sample volume, neutron beam transmission, empty cell signal and detector efficiency as well as normalization to absolute scale ( $\text{cm}^{-1}$ ) was carried out by a standard procedure using the “PASINET” software.

## 2.5 Theoretical investigations with COSMO-RS

Within this contribution, the Conductor-like Screening Model for Realistic Solvation (COSMO-RS [27–29]) was used for the quantification of interactions in solution and for the theoretical investigation of the extraction process of uranyl-nitrate with the *N,N*-dialkylamides: TBP, MOEHA, DEHBA, DEHiBA and DEHDMBA in several organic diluents.

In a nutshell, the COSMO-RS method makes use of the electronic structure of ideally screened molecules in a homogeneously polarizable dielectric continuum and calculates chemical potentials, activity coefficients and free energy-related properties from the statistical thermodynamics of the ensemble of pairwise interacting surface segments of solute-continuum interface (COSMO surface cavity, Fig. 1).

The electronic structures of all molecules in their most relevant minimum energy configurations – and hence, the polarization charge densities on the COSMO surface

cavities around the molecules – can either be taken from the COSMOtherm database or generated by use of quantum chemical DFT-BP86 [30,31]/COSMO [32] calculations with the TURBOMOLE V7.2 [33–35] program package. The extractant structures as well as exemplary COSMO surface cavities can be found in the supplementary information. Beside of the molecule specific distribution of the polarization charge densities on the COSMO surface segments, only the phase composition of the liquid mixture and the system temperature is needed for a COSMO-RS calculation.

After the calculation of activity coefficients, chemical potentials and contact probabilities of all COSMO surface segments, and subsequently, of all molecules in a self-consistent iterative procedure, the COSMO-RS model can be used for the prediction of a broad range of free energy related properties and thermodynamic equilibrium properties.

Within this study, the COSMOtherm program (COSMOtherm, Version 18.0.2), (Eckert, 2014) was mainly used for the prediction of partition coefficients of molecules in infinite dilution between two phases. These partition coefficients can be calculated as the difference of the chemical potentials of the compounds in each of the two phases, and hence, can be interpreted as a measure for the affinity of a compound towards one of the phases. For more information about COSMO-RS theory and other application fields it is referred to literature [29,36–38].

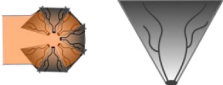

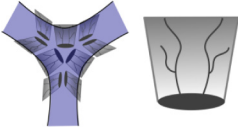
## 2.6 General theory

In this work, we present a minimal model at nanoscale for the prediction of the macroscopic behavior of organic extractant solutions. The term “minimal” means in that context that this model can be used with a minimum of necessary input parameters that are either measurable or have a precise definition and physical meaning. It combines three pioneering works with well-established key elements in colloidal chemistry [39]:

- the concept of pseudo-phases introduced by Shinoda [40] and later used by Tanford [41];
- the expression for the bending free energy of amphiphilic films derived from the works of Ninham [42], Hyde [43,44] and Israelachvili [45];
- classical theories for “living polymers” or “connected worm-like micelles” proposed by Cates [46–48], Lequeux [49], Candau [50] and Khatory [51].

The evolving structure in the organic phase can be seen as made up from four different microphases in chemical equilibrium: endcaps (EC), cylinders (cyl), junctions (J, or equivalently, branching points, BP) and monomeric extractants. These microphases arrange themselves into a colloidal structure. The fourth microphase, monomers, does not significantly contribute to the increase in viscosity. Consequently, its contribution is negligible and is only considered in the context of this model by decreasing the number of molecules participating in the decisive structure. To each of these microphases, an effective packing parameter  $P$  can be defined (cf. Tab. 1). This scalar number is specific for each microphase and represents the

**Table 1.** The three microphases in chemical equilibrium.

Spherical endcaps	Bottlebrush cylinder units surrounding alternating uranyl–nitrate–uranyl chains	Junctions with a saddle-like structure with an average curvature of $H \approx 0$
$P_{EC} = 3$	$P_{cyl} = 2$	$P_j \approx 1.2$
		

geometry that an extractant has to adopt to fit into the interfacial film. The values are estimated from a simple reversion of the effective packing parameters from the aqueous, direct case into the reverse case and probably do not represent the exact limits. The following model and chosen values are rather used to demonstrate and explain the viscosity increase of the organic phase than to obtain quantitative observations. Especially the estimation of the value for junctions is difficult. For junctions, the value of  $P$  is intermediate between the one of cylinders and the one of bilayers, respectively, since they can be regarded as a central bilayer-like region surrounded by three semi-toroidal sections [52]. Therefore, we have set this value to 1.2 for junctions.

Experimental observations from X-ray scattering combined with molecular dynamic simulations have indicated that the organic phase composed of dialkylamides in organic solution tend to form rather a mesoscopic living-network-like structure than spherical aggregates [6]. The main compound are cylinder units composed of alternating uranyl-nitrate chains embodied in a “bottle-brush” structure formed by extractants.

Extraction of uranyl molecules into the organic phase swells the polar core of the present reverse aggregates. Therefore, the mean curvature per extractant and hence, its spontaneous packing parameter  $P_0$ , decreases with increasing uranyl content. With changing  $P_0$  also its differences respective to the effective packing parameter characteristic for each microphase change with uranyl concentration. This difference is used in the following to simulate the evolution of the microphase distribution with increasing uranyl content.

### 2.6.1 Microphase distribution

According to the concept of pseudo-phases, the chemical potential  $\mu$  of a single extractant  $i$  in the diluent is equal to the chemical potential of  $i$  inside a microphase [39–41].

$$\mu_{i,\text{endcaps}} = \mu_{i,\text{cylinders}} = \mu_{i,\text{junction}} = \mu_{i,\text{monomer}}. \quad (1)$$

The local expression of the chemical potential  $\mu_i$  of one extractant in one microphase comprises a standard reference potential  $\mu_i^0$  and a concentration-dependent term  $RT \ln a_i$ , where  $a_i$  is the activity.

$$\mu_{i,\text{endcaps}} = \mu_{i,\text{endcaps}}^0 + RT \ln a_{i,\text{endcaps}} \quad (2)$$

$$\mu_{i,\text{cylinder}} = \mu_{i,\text{cylinder}}^0 + RT \ln a_{i,\text{cylinder}} \quad (3)$$

$$\mu_{i,\text{junction}} = \mu_{i,\text{junction}}^0 + RT \ln a_{i,\text{junction}}. \quad (4)$$

According to concepts by Hyde et al., the bending contribution to the free energy of one extractant in a given microphase can be expressed, by a harmonic approximation, as the deviation of the actual extractant geometry that the extractant must adopt to fit into a highly bent w/o interfacial film. The crucial point is the difference between effective packing in a given sample and the “spontaneous” packing of any given film made of adjacent surface active molecules. All known extractants are oil-soluble and have surface active properties.

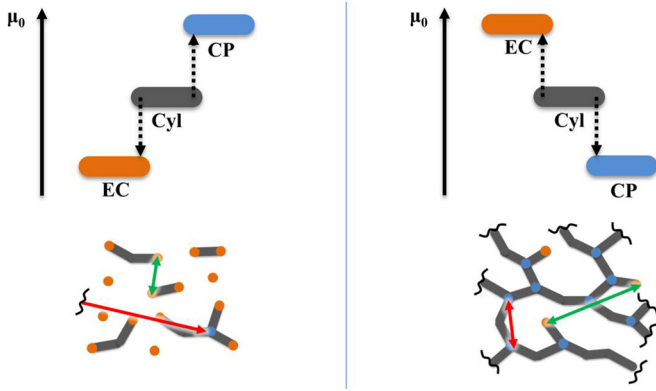
The “frustration” free energy reflects the cost in free energy of packing together interface active molecules under topological constraints. This free energy depends on the difference between the effective packing parameter  $P$  – and the spontaneous packing parameter  $P_0$  – multiplied with a bending constant  $\kappa^*$  [43]. In all of the large number of previously handled cases in the literature, a harmonic expansion of the free energy has shown to be efficient:

$$F_{i,\text{bending}} = \frac{\kappa^*}{2} (P - P_0) \quad (5)$$

with  $P$  denoting the effective packing parameter defined by the shape of a given micro-phase and  $P_0 = (v/a_0 \cdot l)$  denoting the preferred, spontaneous one,  $v$  being the volume of the nonpolar moiety,  $a_0$ , the area per surfactant head-group and  $l$  the mean surfactant chain length. In the case of extractants, the bending modulus  $\kappa^*$  was found to lie in the order of magnitude of 1–2 kT per chain, meaning that the free energy involved in a sphere to cylinder transition is of the order of  $k_B T$  [53,54]. Note that using the Helfrich-Gauss expression of frustration energy thin films is an expansion of equation (5) and moreover would require spontaneous and effective curvature radii to be much larger than chain length: this is never the case in water-poor extracting systems.

In a next step, the evolving structure is considered as built from cylindrical micelles decorated with endcaps and junctions in dynamic equilibrium as defects. Therefore, the standard reference potential of cylinders is defined as a reference state. As a result, the difference in standard





**Fig. 2.** The influence of standard reference chemical potential on microstructure (two extreme cases).

reference chemical potential  $\Delta\mu^0$  of endcaps (EC) and junctions (J) relative to this potential can be derived from the differences of the free energy as a frustration of bending between each microphase of a certain aggregation number  $N_{\text{agg}}$  [39].

$$\begin{aligned} & \mu_{i,\text{EC}}^0 - \mu_{i,\text{cyl}}^0 \\ &= \frac{\kappa^*}{2} \cdot \left[ N_{\text{agg,EC}} (P_{\text{EC}} - P_0(x))^2 - N_{\text{agg,cyl}} (P_{\text{cyl}} - P_0(x))^2 \right] \quad (6) \end{aligned}$$

$$\begin{aligned} & \mu_{i,\text{J}}^0 - \mu_{i,\text{cyl}}^0 \\ &= \frac{\kappa^*}{2} \cdot \left[ N_{\text{agg,J}} (P_{\text{J}} - P_0(x))^2 - N_{\text{agg,cyl}} (P_{\text{cyl}} - P_0(x))^2 \right]. \quad (7) \end{aligned}$$

The spontaneous packing parameter  $P_0$  is varying with the relative uranyl content expressed as the mole fraction  $x = [\text{uranyl}]/[\text{extractant}]$ . Therefore, also the standard reference chemical potentials are dependent on the concentration of complexed uranyl ions in the organic phase. The uranyl content  $x$  varies from  $x=0$ , no uranyl molecules in the organic phase, to  $x \approx 0.45$ , which is the approximate experimental stoichiometry of [Dialkylamide]/[ $\text{UO}_2^{2+}$ ]  $\approx 2.3$  [55,56]. At this value, the organic phase has reached the maximal possible concentration of uranyl nitrate.

The cost in free energy  $\Delta\mu^0$  to convert a cylindrical microphase into an endcap, or respectively, in junction units gives the relative probability of occurrence of each microphase (cf. Fig. 2). Combining equations (2)–(4) and (6) and (7) leads to an expression for the relative concentration of extractants in each microphase ( $c_{i,\text{cyl}}$ ,  $c_{i,\text{EC}}$ ,  $c_{i,\text{J}}$ ).

$$\exp\left(\frac{\mu_{i,\text{EC}}^0 - \mu_{i,\text{cyl}}^0}{RT}\right) = \frac{c_{i,\text{cyl}} \cdot \gamma_{i,\text{cyl}}}{c_{i,\text{EC}} \cdot \gamma_{i,\text{EC}}} \quad (8)$$

$$\exp\left(\frac{\mu_{i,\text{J}}^0 - \mu_{i,\text{cyl}}^0}{RT}\right) = \frac{c_{i,\text{cyl}} \cdot \gamma_{i,\text{cyl}}}{c_{i,\text{J}} \cdot \gamma_{i,\text{J}}} \quad (9)$$

The necessary ratio of activity coefficients  $\gamma_i$  can be derived in a first approximation from the number of extractants per microphase  $N_{\text{agg}}$  as  $\gamma_{i,\text{microphase}} \sim 1/N_{\text{agg,microphase}}$  [39]. The unit used in equations (8) and (9) can be chosen at will: the easiest scale involves concentration in moles, meaning distance are of the order of 1 nm. The molality scale would be more adapted for evaluating entropic corrections, while the mole fraction scale implies delicate “infinitely diluted” reference states that are very far from the electrolyte content in the polar cores of the micelles. In this work, we use the concentration scale for evaluating potentials [57].

Respecting mass conservation, the total concentration of endcap, cylinder and junction units can be calculated from the relative concentrations  $c_{\text{cyl}}/c_{\text{EC}}$  and  $c_{\text{cyl}}/c_{\text{J}}$  and the total concentration of extractants  $c_{\text{Ex}}$  in solution. The total number of extractant molecules per volume  $c_{\text{Ex}}$  is composed of the numbers of extractant  $N_{\text{agg}}$  per cylinder, endcaps and junctions:

$$N_{\text{agg,cyl}} \cdot c_{\text{cyl}} + N_{\text{agg,EC}} \cdot c_{\text{EC}} + N_{\text{agg,J}} \cdot c_{\text{J}} + (c_{\text{monomers}}) = c_{\text{Ex}} \quad (10)$$

$$c_{\text{cyl}} = \frac{c_{\text{Ex}}}{N_{\text{agg,cyl}} + \frac{N_{\text{agg,EC}}}{c_{\text{cyl}}/c_{\text{EC}}} + \frac{N_{\text{agg,J}}}{c_{\text{cyl}}/c_{\text{J}}}} \quad (11)$$

$$c_{\text{EC}} = \frac{c_{\text{cyl}}}{c_{\text{cyl}}/c_{\text{EC}}} \quad (12)$$

$$c_{\text{J}} = \frac{c_{\text{cyl}}}{c_{\text{cyl}}/c_{\text{J}}} \quad (13)$$

Consequently, if the standard reference chemical potential of endcaps is low, the resulting population of endcaps is high. If the standard reference chemical potential of endcaps is high, the formation of endcaps is unfavorable and the resulting concentration is expected to be low (cf. Fig. 2).

As a result, the evolution of the distribution of microphases can be estimated from the evolution of the spontaneous packing parameter  $P_0$  with increasing uranyl concentration.

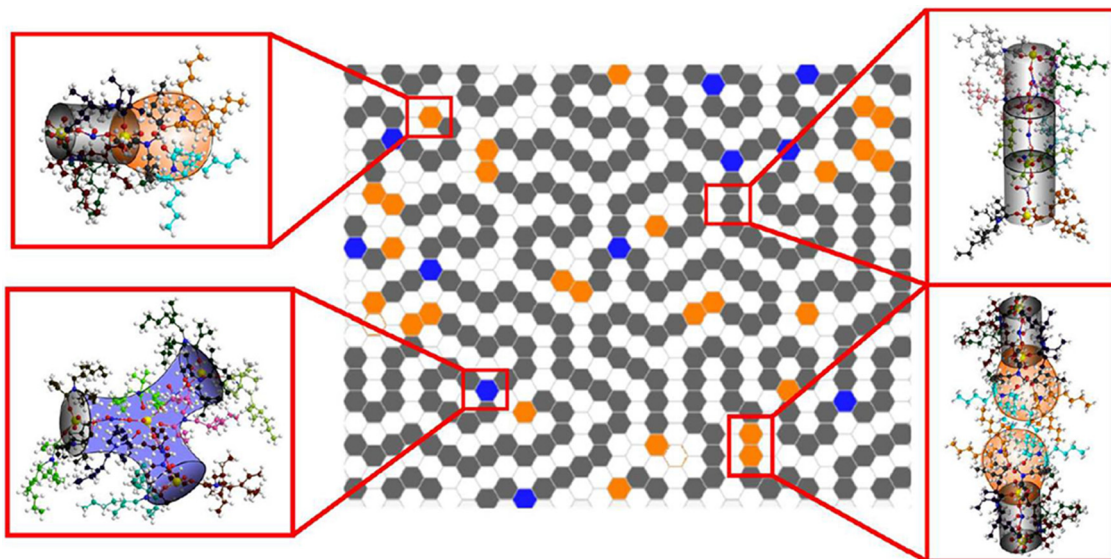
## 2.6.2 Microphase equilibrium controlling viscosity

The microphase distribution that is given by the evolution of the spontaneous packing parameter provides the number of endcaps, cylinders and junctions at a given uranyl concentration and defines the evolving microstructure. We can link this microphase distribution to the macroscopic properties of the system, in specific viscosity.

We consider the following relationship for reptating chains according to Cates [46]:

$$\eta \sim L_{\text{eff}}^3 \quad (14)$$

where  $\eta$  is the zero-shear viscosity of an entangled solution of worm-like micelles and  $L$  is the mean contour length of the micelles. In the case of fast micellar breaking, the



**Fig. 3.** 2D model using an hexagonal grid with endcaps (orange), cylinders (grey) and junction (blue).

scaling exponent is supposed to approach unity [48]. However, the calculated microphase distribution does not give insight into time scales and dynamic aspects of micellar breaking and recombination, and therefore, relaxation regimes of the system cannot be predicted. As a consequence, we must rely primarily on geometrical aspects and length scales [39]. Khatory et al. analyzed the structure of entangled and branched giant micelles [51]. Due to presence of junctions, the contour length  $L$  (endcap to endcap distance in linear micelles without junctions) necessitated a net definition. He defined an averaged total length  $L_{\text{eff}}$  per volume of the structure forming amphiphile that is given by the sum of the respective lengths  $l_i$  of the single microphases multiplied with their corresponding concentration.

$$L_{\text{eff}} = \frac{\left( \frac{c_{\text{EC}}}{2} + c_{\text{cyl}} + c_J \right) \cdot l_{\text{hexagon}}}{c_{\text{EC}} + 2c_J} \quad (15)$$

with  $c_i$  being the concentration of the corresponding microphase.

Since this proportionality is referring to the relative viscosity increase, this  $L^3$  factor has to be scaled with a scaling factor that is considered to be independent of uranyl and extractant concentration, as well as with the concentration dependent zero viscosity of the organic solvent, i.e. the extractant diluted in the diluent with viscosity  $\eta_{\text{dil}}$ . In a first approximation, this viscosity is dependent on the volume fraction of the extractant  $\phi_{\text{ext}}$  according to Einsteins formula [58]:

$$\eta_0 \approx A \cdot \eta_{\text{dil}} (1 + 2.5\phi_{\text{ext}}) \quad (16)$$

with  $A$  being a scaling factor. In this example, this scaling factor has to be chosen to be  $1/12$  [mPa·s] to fit the experimental viscosity curve.

### 2.6.3 Towards a two-dimensional picture of the organic phase

Knowing the number distribution of endcap, cylinder and junction units in a fixed volume at a certain metal concentration allows creating an intuition-driving, two-dimensional image of the microstructure morphology at mesoscale. A three-dimensional modeling would be much more difficult to implement, with no great increase in intuitive capture of the mechanism. So, we decided to make a 2D model using a quasi-metropolis algorithm. For this purpose, a hexagonal grid is filled randomly with microphases according to their relative distribution [59]. The total fraction of hexagons on the grid filled by a microphase represents the volume fraction of extractant. One hexagon either represents one microphase or solvent.

In a second step, the structure in two dimensions is optimized based on a minimization of “mismatch” energy with a Monte-Carlo-like algorithm. The “mismatch” of one microphase represented in 2D by a hexagonal lattice is defined as follows: one imagine any water-domain as build from three types of elements: those with one (endcaps), those with two (cylinders) and those with three (junctions) binding sites to neighboring elements (cf. Fig. 3). These elements are “matching” when they correspond to continuity of water cores. A “mismatch” occurs when the rules defining the connection within a microphase are not satisfied.

An endcap shows no mismatch, when only one further microphase is in the neighboring 6 hexagons. When it is more or less, the amount of mismatch energy in the sample is calculated by:

$$F_{\text{frust,EC}} = |N_{\text{EC}} + N_{\text{cyl}} + NJ - 1| \quad (17)$$

with  $N_{\text{EC}}$ ,  $N_{\text{cyl}}$  and  $N_{\text{CP}}$  being the number of direct adjacent endcaps, cylinders and branching points, respectively.

An exemption is made for the possibility of bridging endcaps that are expected to result in positive wetting energy end entropy gain by fluctuating uranyl molecules. In that case, an endcap is allowed to exhibit two neighboring microphases.

A cylinder is matched when two further microphases adjoin. Furthermore, a steric requirement has to be fulfilled. The resulting cylinder chain has to form an angle between  $120^\circ$  and  $240^\circ$ . If the cylinder has more or less neighbors, the corresponding mismatch energy can be calculated via:

$$F_{\text{frust,cyl}} = |N_{\text{EC}} + N_{\text{cyl}} + N_{\text{J}} - 2|. \quad (18)$$

A junction however induces no mismatch energy when exactly three microphases are in the neighboring three hexagons. Moreover, also for junctions, steric conditions have to be fulfilled, leading to a  $120^\circ$ -angle between each microphase. It was reflected, if a junction–junction interaction is favorable or not. We decided that it is, especially at higher extractant and branching point concentration. Making this interaction unfavorable did not lead to structures with a lower occurrence of mismatches. In addition, it was indicated in literature that there is an attractive force between junctions that can lead to phase separation [60,61]. This picture was recently completed with the proof of presence of nanocapillarity [62]. Therefore, the total mismatch can be calculated in the following way:

$$F_{\text{frust,J}} = |N_{\text{EC}} + N_{\text{cyl}} + N_{\text{J}} - 3|. \quad (19)$$

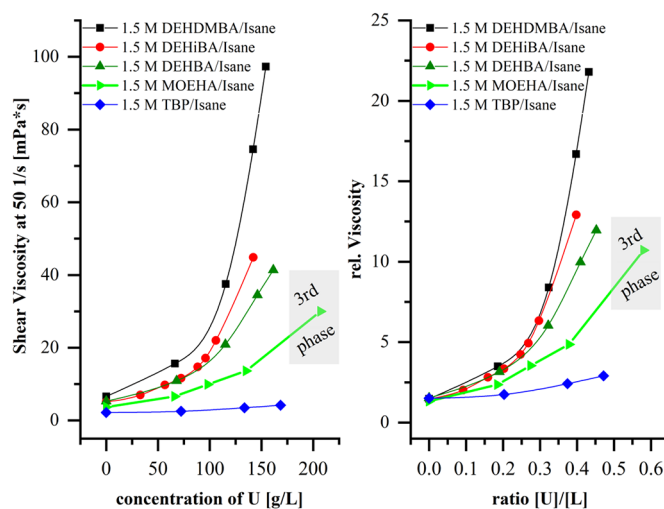
### 3 Results and discussion

In the following, a number of selected experimental observations is presented and discussed. Furthermore, the qualitative trends are discussed in terms of a minimal model at nanoscale considering the chemical terms at molecular scale, the physical terms at mesoscale and the fluid mechanical terms at macroscale.

#### 3.1 Experimental observations

##### 3.1.1 Viscosity increase with decreasing spontaneous packing parameter

Figure 4 shows the influence of the extractant on the viscosity of the organic phase. Each organic phase contains 1.5 M extractant diluted in Isane IP 175, a mixture of alkanes with isoparaffinic structure (C10–C12). The viscosity increases for each organic phase with increasing uranyl concentration. A significant difference is observed in the behavior of the five investigated extractants. The viscosities are plotted on absolute scale against the mass concentration of uranyl as well as in reduced scale. For that, the viscosity was normalized by the viscosity of the extractant/diluent mixture before contact with the aqueous phase. As can be noticed, the viscosity normalized to the non-contacted solvent is not 1, but approximately 2 at  $x=0$ . That shows that the viscosity already increases by



**Fig. 4.** Viscosity increase due to increasing uranyl concentration in the organic phase for different extractants at  $25^\circ\text{C}$ . Left: apparent viscosity at a shear rate of  $50 \text{ 1/s}$ . Right: relative viscosity normalized by the viscosity of the non-contacted extractant/diluent mixtures. ■ 1.5 M DEHD MBA, ● 1.5 M DEHi BA, ▲ 1.5 M DEH BA, ► 1.5 M MOE HA, ◆ 1.5 M TBP diluted in Isane IP 175 versus the molar ratio uranyl/extractant.

a factor of 2 after contact with an aqueous phase with 3 M nitric acid. The uranyl concentration was normalized by uranyl/extractant mol ratio and covers the range from 0 to approximately 0.5, the stoichiometrical limit in uranyl capacity of the organic phase. The extent of the viscosity increase rises in the order  $\text{TBP} < \text{MOEHA} < \text{DEHBA} < \text{DEHiBA} < \text{DEHD MBA}$ . While the viscosity of the organic phases containing TBP increases almost linearly by a factor of 3 the viscosity of the organic phase based on DEHD MBA rises exponentially by a factor of 23 comparing the non-contacted fluid and the maximal loaded organic phase.

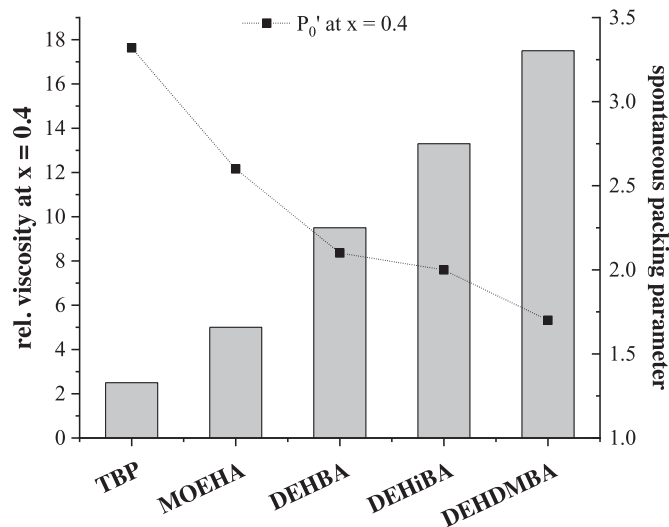
Due to the high volume fraction of extractant in the organic phase, determination of the spontaneous packing parameter by combined small-angle neutron and X-ray scattering is difficult. Therefore, we have developed a procedure that allows estimating the spontaneous packing parameter of an extractant purely from molecular structure and molar volume. This procedure is explained in the supplementary information.

Figure 5 shows the correlation of this calculated spontaneous packing parameter with experimental observed viscosity at  $x=0.4$ . There is a strong link between observed viscosity and spontaneous packing parameter. To our knowledge, this link between induced viscosity and spontaneous packing variation with and without complexation has neither been considered in literature for any of the surface-active extractants heavily used in hydrometallurgy.

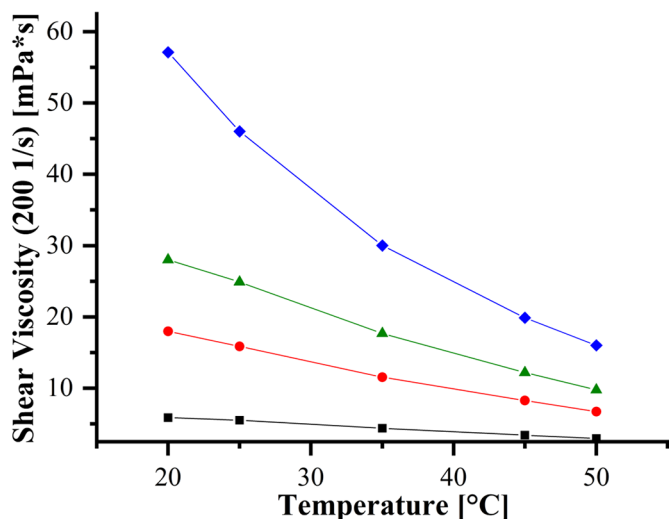
##### 3.1.2 Temperature dependence

In the following investigations we will focus on the extractant DEHiBA. Figure 6 shows the temperature



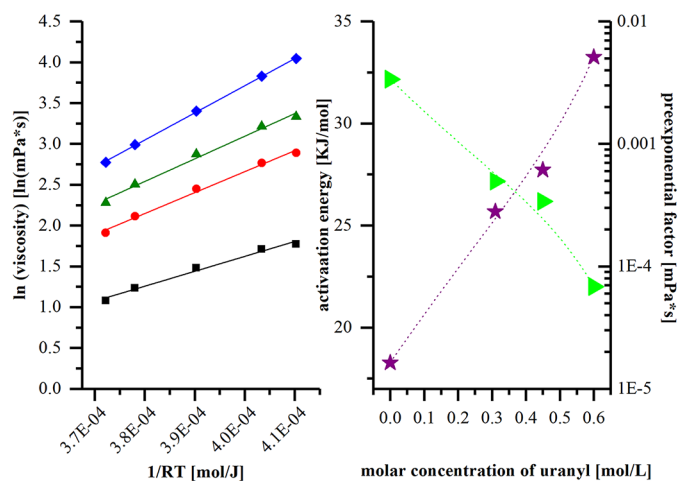


**Fig. 5.** Correlation between the spontaneous packing parameters estimated from geometry and the observed viscosity (in grey, cf. Fig. 4). For illustration, the viscosity of TBP, MOEHA, DEHBA, DEHiBA and DEHDMBA is shown at a uranyl content of  $x = [\text{uranyl}]/[\text{Ex}] = 0.4$ . The estimation of the spontaneous packing parameter is explained in the supplementary information.



**Fig. 6.** Temperature dependence of shear viscosities (200 1/s) of organic phases (1.5 M DEHiBA/Isane) as a function of uranyl content. Color code: 0.60 M uranyl (blue), 0.45 M uranyl (green), 0.31 M uranyl (red), 0 M uranyl (black).

dependence of the viscosity of 1.5 M DEHiBA in Isane at different uranyl concentrations. The viscosity decreases with increasing temperature and is most elevated for the system containing the highest uranyl concentration. For a quantification of this observation, the temperature dependence was fitted with the simple Arrhenius equation, whose application on liquid viscosity was first attributed to de Guzman, but popularized by Andrade [63]. Now the equation is used to fit viscosity data of small molecules but



**Fig. 7.** Left: linear fits using equation (55) for 1.5 M DEHiBA diluted in Isane IP 175 charged with  $\blacksquare$  0 M  $\bullet$  0.31 M  $\blacktriangle$  0.45 M  $\blacklozenge$  0.6 M Uranyl. Right: resulting fit parameter from Arrhenius fits;  $\blacktriangleright$  preexponential factor,  $\blackstar$  activation energy.

also polymers.

$$\eta = A \cdot \exp\left(\frac{E_A}{RT}\right) \quad (20)$$

$$\ln \eta = \ln A + E_A \cdot \frac{1}{RT}. \quad (21)$$

In the Arrhenius equation for liquid viscosity (Eq. (20)), the preexponential factor is correlated to contributions due to disorder, entropy and motion [64]. Another interpretation is also to see the parameter  $A$  as the viscosity at infinite temperature [64],  $\eta_\infty$ . The parameter  $E_A$  is related to a certain activation energy that is needed for viscous flow [64,65].

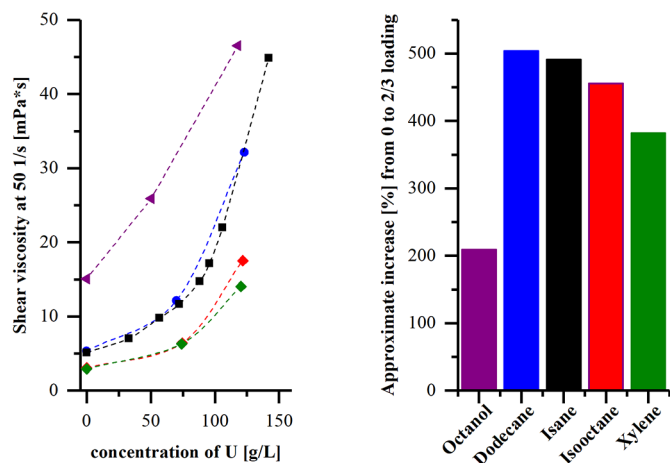
As can be seen in Figure 7, the activation energy for viscous flow increases with increasing uranyl concentration. In contrast hereto, the preexponential factor  $A$  decreases with increasing uranyl concentration. As a result, the higher the uranyl content, the more activation energy is needed for viscous flow at a certain temperature, while the parameter  $A$ , a factor describing the entropical contribution decreases. This observation indicates a more pronounced mesoscopic organization at higher uranyl concentration.

### 3.1.3 Diluent dependence

Figure 8 shows the dependence of the viscosity evolution of 1.5 M DEHiBA diluted in different diluents. The absolute values are shown as well as the relative increase from  $x=0$  to  $x=0.33$ . A significant dependence on the viscosity is observed. The viscosity increase from  $x=0$  to  $x=0.33$  rises in the order octanol < xylene < isooctane < Isane < dodecane, thus with increasing penetration power of the diluent [66]. This observation is consistent with the result described above that the viscosity increase depends on the spontaneous packing parameter. A penetrating diluent can

**Table 2.** COSMO-RS predicted infinite dilution partition coefficients of a diluent molecule  $i$  between a pure extractant and a pure diluent phase. All calculations were performed on the BP-TZVPD-FINE level at a temperature of 25 °C with 7 conformers for TBP, 8 conformers for MOEHA, 9 conformers for DEHBA, 4 conformers for DEHiBA and 11 conformers for DEHDMBA. In order to calculate the thermodynamic partitioning, the volume fraction of both phases was set to unity.

	Extractant				
	TBP	MOEHA	DEHBA	DEHiBA	DEHDMBA
1-octanol	−0.3268	−0.3261	−0.3922	−0.3265	−0.1135
1,3-dimethylbenzene	−0.0840	−0.1106	−0.1356	−0.1307	−0.1216
2,2,4-trimethylpentane	0.2761	0.1267	0.0503	0.0579	0.0336
2,2,4,6,6-pentamethylheptane	0.4010	0.2147	0.1234	0.1375	0.1063
dodecane	0.5273	0.2915	0.1827	0.1990	0.1603



**Fig. 8.** Left: shear viscosities at 25 °C dependent on diluent and uranyl concentration. Investigated system: 1.5 M DEHiBA in different diluents contacted with different aqueous phases (uranyl nitrate dissolved in 3 M nitric acid). Right: approximate viscosity increase from contact with nitric acid (0 M) to 2/3 loading of the organic phase ( $\approx 0.5$  M uranyl).

swell the apolar extractant volume and consequently increase the spontaneous packing parameter [66]. The role of octanol in this investigation is under discussion. Due to its polar moiety, octanol can participate actively in aggregation processes and even self-aggregate [67–70]. Therefore, this effect cannot be exclusively contributed to octanol penetration.

As an indicator for the propensity of a diluent to interact with extractant molecules and hence, for the penetration power of a diluent into the protruding extractant chains, COSMO-RS predicted infinite dilution partition coefficients of a diluent molecule between a pure extractant and a pure solvent phase can be used.

$$\log_{10}(P_i^{E,D}) = \log_{10} \left[ \exp \left( \frac{-\left(\mu_i^{(E)} - \mu_i^{(D)}\right)}{RT} \right) \frac{V_D}{V_E} \right] \quad (22)$$

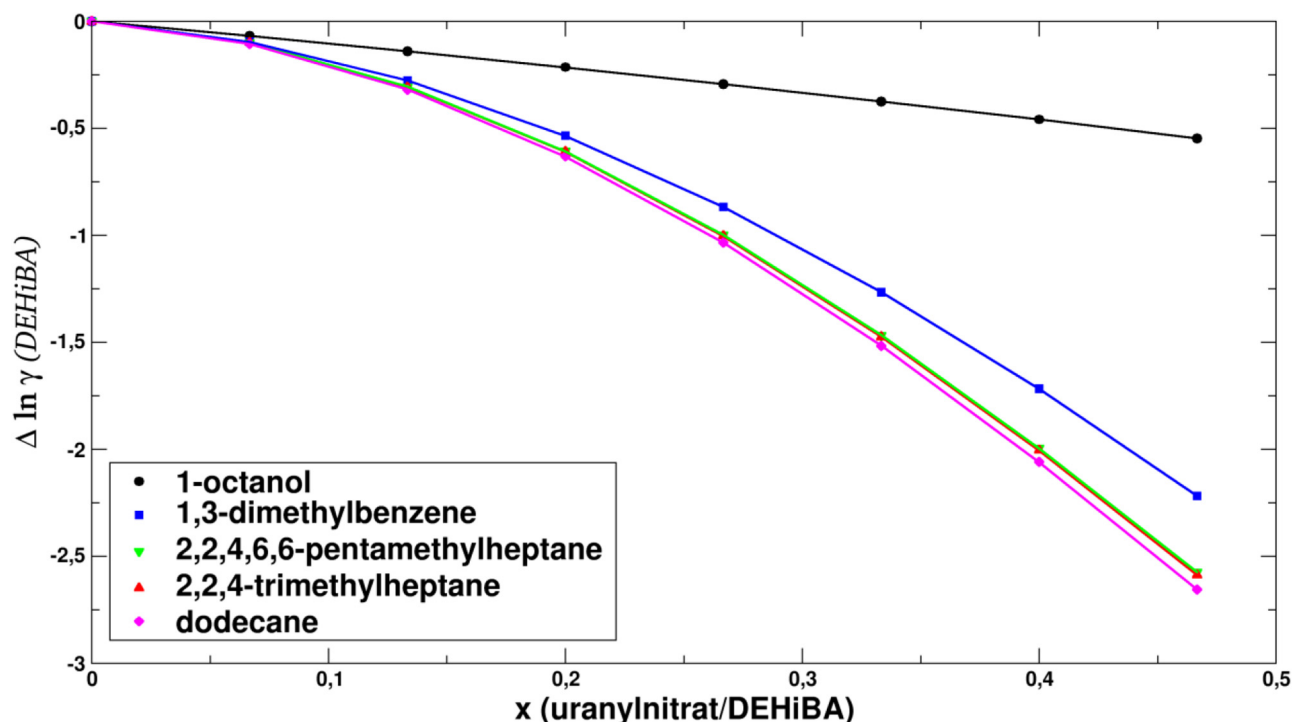
Within the COSMO-RS model, the partition coefficient  $\log_{10}(P_i^{E,D})$  of a diluent  $i$  between a pure extractant and a pure diluent phase can be calculated from the infinite dilution chemical potentials of the diluent  $i$  in the corresponding phases. Hence, the  $\log_{10}(P_i^{E,D})$  values do not only indicate the propensity of the diluent  $i$  to interact with extractant molecules, but can also be used to evaluate and compare the influence of different diluents on a chosen extractant, as it is shown in Table 2. Note that the results for the extractant DEHiBA are in good agreement with the expected penetration power and with the order of the diluents: octanol < xylene < *isooctane* < pentamethylheptane < dodecane (see also Fig. 6).

The lower the  $\log_{10}(P_i^{E,D})$  values for a chosen extractant, the higher the propensity of the diluent molecules to interact with the extractant, therefore the tendency to “wet” the extractant chains and swell the apolar part. Another interesting trend can be seen from the comparison of the  $\log_{10}(P_i^{E,D})$  values for dodecane with changing extractants: here, the values of the partition coefficients also decrease with decreasing fraction of polar molecular surfaces in the order TBP > MOEHA > DEHiBA > DEHBA > DEHDMBA.

In order to evaluate the influence of uranyl addition to the extractant diluent system, COSMO-RS predicted logarithmic activity coefficients of an extractant ( $\Delta \ln \gamma_i$ ), or more precisely, the deviation of the logarithmic activity coefficient of an extractant in a uranyl nitrate containing diluent with respect to a reference system without uranyl ( $\Delta \ln \gamma_i$ ) can be analyzed.

$$\ln \gamma_i = \frac{\mu_i^{(X)} - \mu_i^{(pure)}}{RT} \quad \text{and} \quad \Delta \ln \gamma_i = \frac{\mu_i^{(ref+U)} - \mu_i^{(ref)}}{RT}. \quad (23)$$

The COSMO-RS predicted  $\Delta \ln \gamma_i$  values are directly related to the difference of the chemical potentials of an extractant in a system with and without uranyl nitrate and thus also dependent on the uranyl nitrate content in the mixture system. From the results of different extractant-diluent combination we learned that the chemical potentials of the extractant in the uranyl nitrate containing system is always lower than the corresponding chemical



**Fig. 9.** Deviation of COSMO-RS predicted logarithmic activity coefficients of DEHiBA in different diluents with uranyl nitrate from the corresponding reference systems without uranyl nitrate. All calculations were performed on the BP-TZVPD-FINE level at a temperature of 25 °C with 4 conformers of DEHiBA and extractant concentrations of 1.5 mol DEHiBA per liter of diluent.

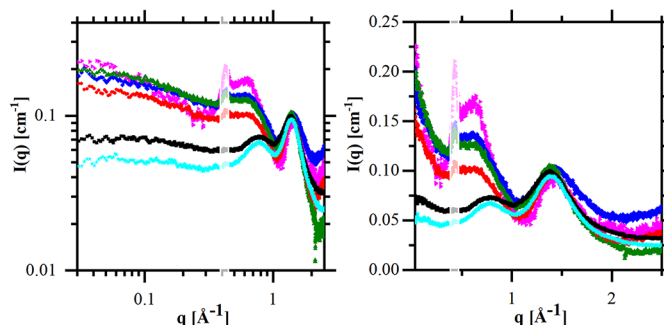
potentials in the system in absence of uranyl nitrate. However, the extent of the deviation from the reference system is strongly dependent on the diluent and again follows the order: octanol < xylene < *isooctane* < pentamethylheptane < dodecane, as it is shown in Figure 9.

### 3.1.4 Scattering results

X-ray scattering was measured for organic phases containing 1.5 M DEHiBA diluted in Isane and increasing uranyl concentration. The resulting spectra are shown in Figure 10. The spectra can be separated into different characteristic regions.

- At high  $q$  ( $1.4 \text{ \AA}^{-1}$ ), a solvent peak is observed for all solvents containing mainly saturated hydrocarbon chains. It is attributed to the local correlations of carbons in neighboring alkyl chains of diluent and/or extractant. In all cases, this peak is broad indicating the absence of crystallinity in the solvent (diluent).
- In the middle  $q$  range, a broad hump evolves for all of the spectra. At low uranyl concentration (0 and 0.04 M) the peak evolves at a  $q$ -value of  $0.77 \text{ \AA}^{-1}$  which corresponds to a correlation between electron-rich centers in a distance of around  $8.2 \text{ \AA}$ . It indicates a structured organic solution even after contact with nitric acid.

The situation changes profoundly when more uranyl is present in the organic solutions. The correlation hump is shifted towards lower  $q$ , indicating that the correlation distance between two electron-rich regions increases. The



**Fig. 10.** SAXS spectra of organic phases containing 1.5 M DEHiBA dissolved in Isane IP 175 and charged with  $\star$  0 M  $\blacksquare$  0.04 M  $\bullet$  0.24 M  $\blacktriangle$  0.30 M  $\blacklozenge$  0.37 M  $\blacktriangleright$  0.61 M uranyl by contact with aqueous phases. Left: logarithmic scale; right: linear scale.

hump maximum is found at  $q^* = 0.64 \text{ \AA}^{-1}$  ( $2\pi/q^* = 9.8 \text{ \AA}$ ) and does not change within a deviation of  $\pm 0.2 \text{ \AA}$ . Since at higher uranyl concentration, uranyl molecules are the scatterers with by far the highest electron density and since this correlation hump increases with uranyl concentration, we can safely attribute to the correlation between two uranyl ions. This indicates that the uranyl ions are not homogeneously distributed within the polar core of the present structure. Moreover, since the peak is broad, the distance between nearest neighbor uranyl must fluctuate with time. The actinides rather keep a definite mean distance of  $9.8 \pm 0.2 \text{ \AA}$ . A possible

explanation for this phenomenon is the presence of uranyl-nitrate-uranyl chains, as one-dimensional ionic liquids. These were also already observed by molecular dynamic simulations by Rodrigues et al. in heptane [6]. The fact, that this hump is quite broad indicates the presence of vacancies within these one-dimensional chains, or respectively, this network or a mixture of different structures. As pointed out in the paragraph before, at higher extractant concentration, wetting energies can take place, facilitating endcap-endcap bridges.

- The peak at  $0.43 \text{ \AA}^{-1}$  corresponds to the Kapton window which is not sufficiently subtracted due to the low transmission values of the sample (close to 4% for the most concentrated samples caused by adsorption due to uranyl even at 17 keV). Therefore, within the range from  $0.37$  to  $0.47 \text{ \AA}^{-1}$  must be ignored and is only plotted as slightly visible.
- The region at low  $q$  is difficult to interpret since a strong structure factor is expected that overlaps the form factor [71]. The curves are almost flat (slopes of  $-0.2$  to  $-0.5$ ). That means the scattering of the microstructure is homogeneous for length scales above 4 nm. There are two possibilities that result in this scattering pattern:
  - First, the self-assembly results in a mesh of a certain size, thus ensuring homogeneity at large scale [72]. This is also favored by molecular dynamics [6].
  - The second possibility is that the structure is quite polydisperse composed of small and larger aggregates resulting in a structure that is homogeneous in average, which would result in an Ornstein-Zernike behavior damped at low- $q$  by sterical repulsive effects.

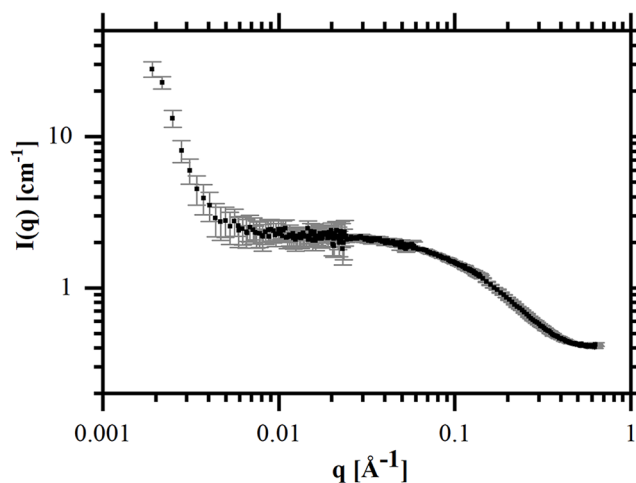
Furthermore, it is not obvious that the sample is exempt from long range heterogeneities. When connection points assemble in bundles that can transform in a small liquid crystal, the regime is “Onsager regime” [73].

Therefore, the behavior at very low  $q$  was checked for the samples suspected on having branching points. The effective attraction between branching points has received lots of attention recently, as “nanocapillarity” [62]. Therefore, a sample containing 1.5 M DEHBA in deuterated dodecane and at an elevated uranyl concentration of 0.5 M was thoroughly examined. The result is shown in Figure 11. For this sample, a steep low- $q$  scattering is observed below  $q = 0.04 \text{ \AA}^{-1}$ . After the plateau, the curve rises with a slope close to  $q^{-4}$ , namely  $q^{-3.8}$ . This increase can have different origins. The most probable explanation is the formation of a large mesoscopic structure with a well-defined interface that is the origin of the quasi-Porod decay at low angles. This sample is clearly in the Onsager regime [74].

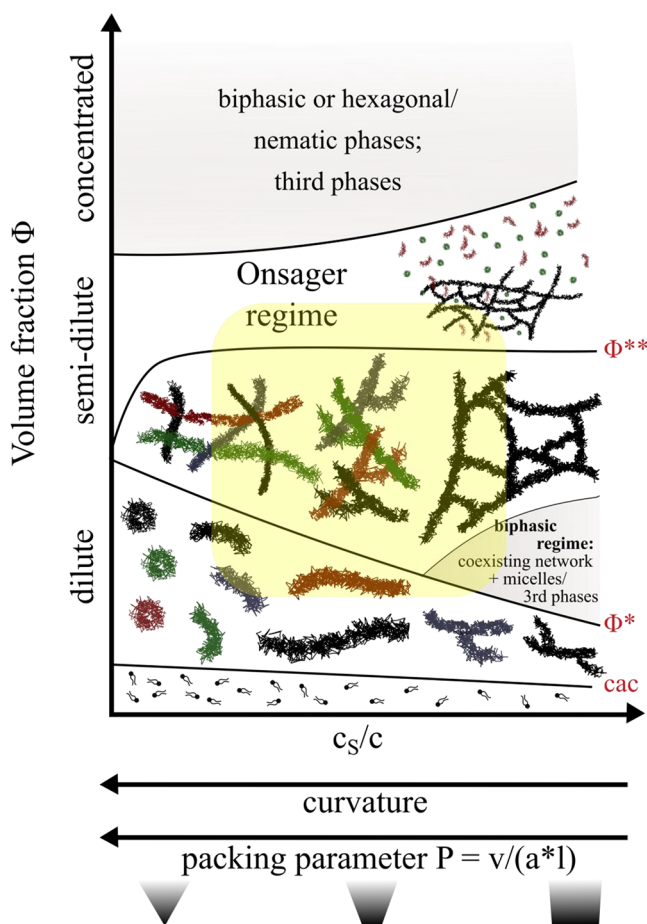
The typical size is larger than 160 nm, due to the order of magnitude they could be called nanocrystals. Most likely it is an Onsager regime (cf. Fig. 12), when connection point regroup in larger superstructures [59].

### 3.2 A minimal model to explain and predict the viscosity increase

From the experimental observations described above, we conclude that the origin of the viscosity increase of the

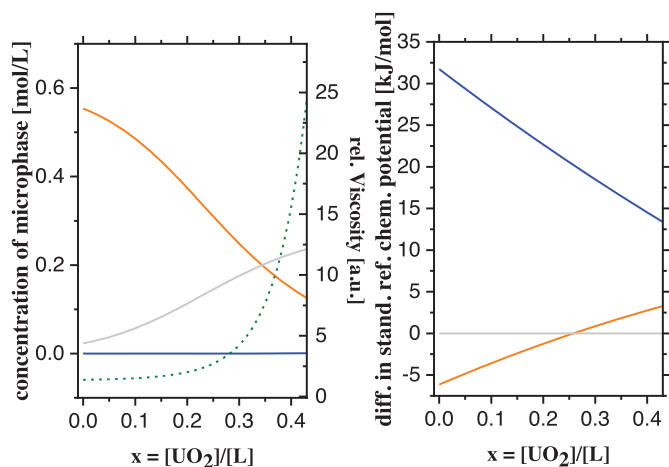


**Fig. 11.** Example of a rise in low  $q$  as seen for some of the samples. This present example was measured with 1.5 M DEHBA diluted in deuterated dodecane charged with 0.5 M uranyl. In grey the error bars are presented.



**Fig. 12.** Schematic view of the different regimes of gelation for concentrated cylinders. Replotted and adjusted from [48]. The microstructure depends both on the volume fraction and the metal concentration determining the spontaneous curvature of the extractant. In yellow, the most probable concentration range is indicated.





**Fig. 13.** Left: evolution of the microphase distribution and simulated viscosity as a function of the uranyl concentration. Right: difference in standard reference chemical potential respective to cylinders as reference state. Color code: orange: endcaps, grey: cylinders, blue: junctions, black experimental values. For this example, the following input parameters were used:  $P_0(x=0) = 2.8$ ;  $P_0(x=0.43) = 2.2$ ;  $c(\text{Ex}) = 1.2 \text{ M}$ ;  $\kappa^* = 2 \text{ kT/extractant}$ .

organic phase can be attributed to a structuration at nanoscale that is more and more pronounced when the uranyl concentration is increased. We propose to describe the evolving structure as the formation of a three-dimensional living network composed of a one-dimensional ionic liquid of alternating uranyl-nitrate chains embodied in a “bottlebrush” structure formed by extractants. Our new thermodynamic model describes the evolving structures as built by cylinder units with endcaps and junction as defects.

### 3.2.1 Microphase distribution and relative viscosity

In the following, this minimal model is applied on a model system to demonstrate the principle. The complexation of uranyl ions leads to an increase of the polar core radius, thus to an increase of the area per extractant at the interface between the polar core and the apolar chains protruding into the organic diluent. Therefore, the spontaneous packing parameter decreases from  $P_{0,\text{init}}$  at  $x=0$  to  $P_{0,\text{max}}$  at  $x=0.45$  as a function of the uranyl content. For this example, we consider a system where the spontaneous packing parameter varies linearly from 2.8 to 2.2. The resulting evolution of  $P_0$  was used to calculate the cost in free energy to form endcaps or junctions respective to cylinders that we defined as the reference state (Fig. 13, right). The cost in free energy to form endcaps from cylinders increases continuously. As a consequence, endcaps become less and less favorable. Cylinders and junctions, on the other hand, become energetically more favorable with increasing uranyl concentration. The cost in free energy gives the microphase distribution of endcaps, cylinders and junctions with as a function of the uranyl concentration and can be transferred into a relative viscosity by introducing the effective length  $L_{\text{eff}}$  (Fig. 13, left).

As can be seen, the concentration of endcaps decreases continuously with increasing uranyl concentration. The concentration of cylinders increases gradually and becomes dominant for concentrations larger than  $x=0.3$ . Although the cost in free energy to form junctions decreases significantly with increasing uranyl concentration, the concentration of junctions stays low. This is due to the higher number of extractants are needed to form a junction (5-6) than to form an endcap (1-2) or a cylinder (3-4). Therefore, the concentration of junctions does not become high enough to induce a reduction of the relative viscosity as it is the case e.g. the case for aqueous solutions of anionic surfactants in presence of salt [75]. As a consequence, the viscosity increases exponentially with increasing uranyl concentration, as it is observed experimentally.

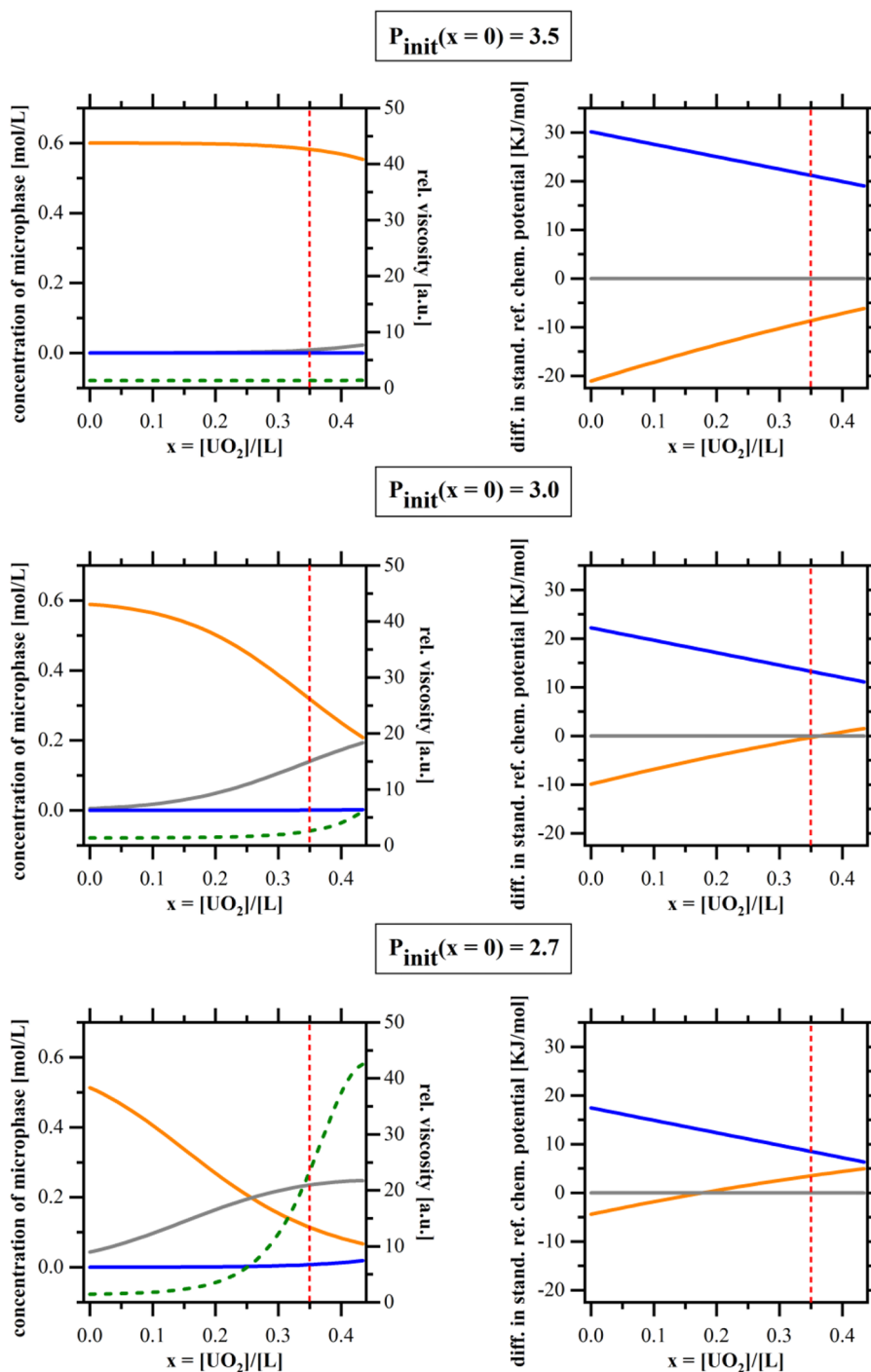
### 3.2.2 Variation of the spontaneous packing parameter

The experimental observations have shown that the extent of the viscosity increase strongly depends on the spontaneous packing parameter. In order to show this dependence by use of the new thermodynamic model introduced in this work, we compare three model systems. The spontaneous packing parameter of each system varies by a value of  $\Delta P_0 = 0.7$  from  $P_{0,\text{init}}$  at  $x=0$  to  $P_{0,\text{max}}$  at  $x=0.45$ . The only parameter that changes is  $P_{0,\text{init}}$ , the initial, spontaneous packing parameter in absence of uranyl nitrate.

Figure 14 shows the evolution of microphase distribution and viscosity by changing the extractant geometry from a curved to a less curved one.

For all three model systems, the microphase distribution changes in the way described above, however in different extent. For the curved extractant ( $P_{0,\text{init}} = 3.5$ ), endcaps are always the dominant microphase independent of the uranyl concentration in the system, while for the medium curved extractant ( $P_{0,\text{init}} = 3.0$ ), cylinders become dominant at high uranyl concentration and for the least curved extractant ( $P_{0,\text{init}} = 2.5$ ), cylinders are dominant above  $x=0.2$ . In all three cases, the concentration of junctions increases with increasing uranyl concentration, but stays low, thus not inducing a viscosity increase due to the presence of additional stress relaxation points. As a consequence, the simulated relative viscosity increases with decreasing initial spontaneous packing parameter and differs up to a factor of 30 in this example.

Using a Monte-Carlo-like approach, the microphase distribution can be transferred into a two-dimensional image representing a snapshot of the microstructure of the organic phase at a given uranyl concentration. The results from the simulations at  $x=0.35$  are shown in Figure 15 and indicate that a higher concentration of endcaps, originating from a more curved extractant, induces shorter aggregates. Therefore, the aggregate length increases with decreasing spontaneous packing parameter and consequently increases the viscosity. This simple series of simulations gives first insight in the origin of the viscosity increase of extractant-rich organic solvents in presence of heavy metals.

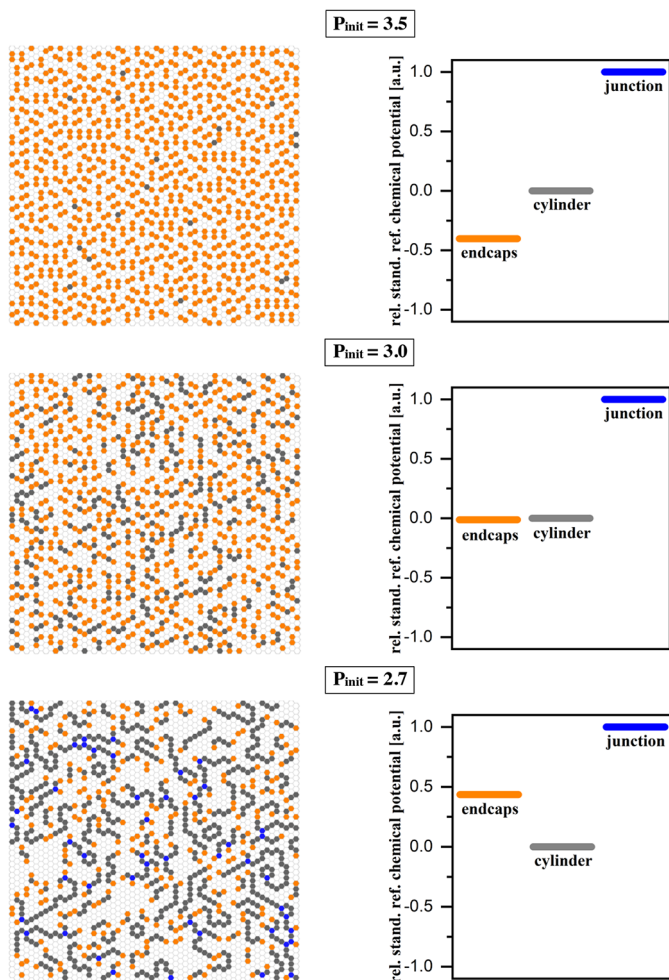


**Fig. 14.** Calculated microphase distribution of endcaps (orange), cylinders (grey) and junctions (blue) as well as the corresponding differences in standard reference chemical potential respective to cylinders dependent on the initial spontaneous packing parameter  $P_{\text{init}}$  and the uranyl content  $x$ . The calculated relative viscosity curve is shown in as dashed green line. The relative decrease of the initial spontaneous packing parameter from  $x=0$  to  $x=0.45$  was set to  $\Delta P_0 = 0.7$ . The total extraction concentration was chosen to be 1.2 M and the bending constant  $\kappa^* = 2 \text{ kT/extractant}$ . The position of the Monte-Carlo-like simulation shown in [Figure 15](#) is indicated by a red dashed line.

### 3.2.3 Possibility of Onsager transition

[Figure 16](#) shows the structural evolution dependent on the initial spontaneous packing parameter and the volume fraction of extractant molecules. A structural change with

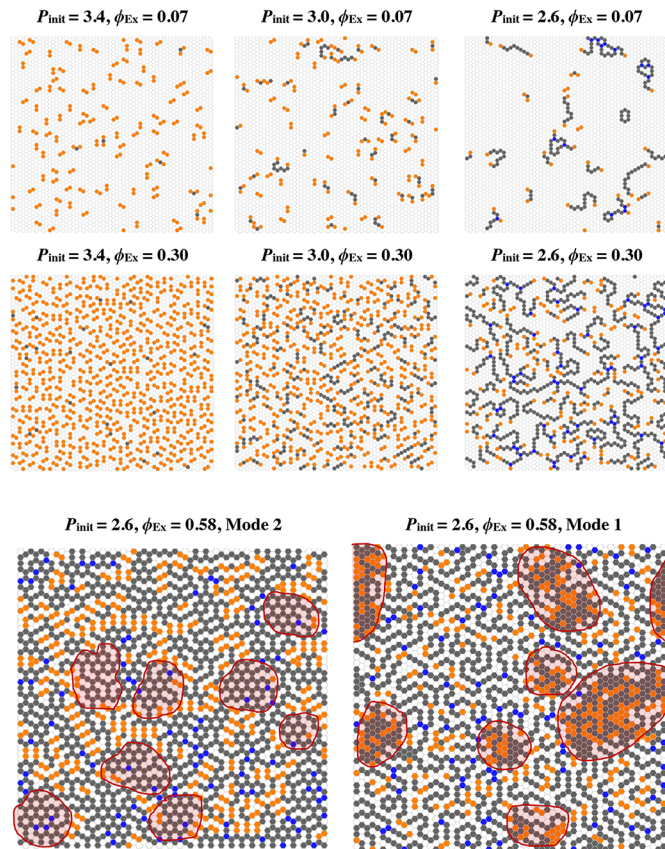
concentration can be observed. First, with increasing volume fraction of aggregated extractants, the aggregates come closer together and the probability of an interaction as well as a collision of the resulting aggregates is higher. Second, one can also see that the probability of



**Fig. 15.** Two-dimensional image of the organic phase and rel. standard reference chemical potential at  $x=0.35$  with different initial spontaneous packing parameters  $P_{\text{init}}$ . The structural composition and the corresponding microphase distribution are shown in Figure 14.

“bridging endcaps” and scattered larger aggregates seems to increase – especially when junctions are present. Furthermore, it should be noted that the attraction between cylinders is stronger than between spheres [76]. Therefore, this transition is also favored by the predominance of cylinders when the spontaneous packing parameter is decreased.

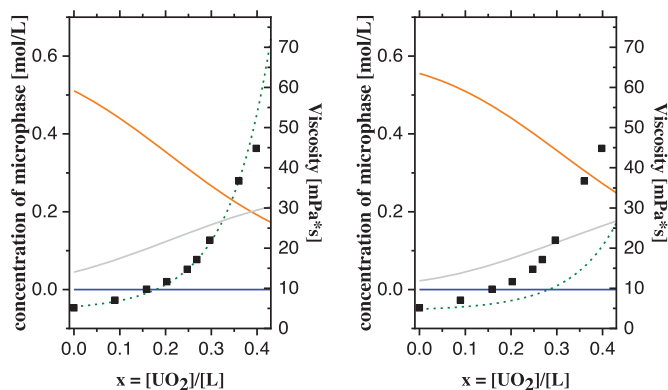
Moreover, Figure 16 also indicates that at elevated extractant concentration, it is more difficult for the system to form a microstructure in which a minimum of mismatched microphases are present. For the two-dimensional investigation, this transition starts above approximately 50 volume percent of extractants forming aggregates. For the three-dimensional case, this value can differ since a three-dimensional arrangement can offer more structural freedom. If this limiting volume fraction is reached, the microstructure must split into regions with high mismatch (marked in red) and regions with less mismatch, in order to minimize the total mismatch energy of given configuration [60,61,73]. In order to point out this phase separation, the



**Fig. 16.** Two-dimensional image derived from Monte-Carlo-like simulation dependent on the initial packing parameter and the volume fraction of aggregated extractant. Calculations were carried out at  $x=[U]/[Ex]=0.35$  and the bending constant was set to  $\kappa^*=2 k_B T/\text{extractant}$ . Below, the simulation was carried out in two different ways to point out the Onsager transition. Mode 2 describes the general procedure used in simulations above, where the total mismatch of the system is minimized. Minimization by Mode 1 minimizes the number of mismatches, in order to point out the regions of strong mismatch free energy.

resulting microstructure was optimized for the case of a relatively low curved extractant ( $P_{\text{init}}=2.6$ ) in two ways: in the left figure, the total mismatch energy of the system is minimized as it was done for the Monte-Carlo-like simulations before. In the right figure, the microstructure was optimized in a way that the number of mismatch in a given configuration was minimized. For this second case, the resulting “clouds” of mismatched microphases are more visible and the term “nanocrystals” is more traceable. If these “clouds” are small enough, the organic phase appears as a macroscopic homogeneous phase. This state is called the “Onsager regime”. If the “clouds” grow big enough, macroscopic phase separation within the organic phase into an extractant-rich and an extractant-poor phase will occur. Therefore, this mechanism can be considered as an efficient way of nucleating the formation of third phase [77]. We stress here that this “nanocapillarity” mechanism involving connection of domains is linked to coalescence and has nothing to do with condensation via a sticky sphere potential.





**Fig. 17.** Left: simulated (green dashed) and experimental viscosity (black spheres) of 1.5 M DEHiBA applying a variation of the spontaneous packing parameter from 2.6 to 2.0,  $\kappa^* = 3 \text{ kT}$ /extractant and an effective extractant concentration of 1.2 M. Right: simulated viscosity (green dotted) applying additionally a solvent penetration of 3%. For both cases, additionally the microphase distribution of end-caps (orange), cylinders (grey) and junctions (blue) is shown.

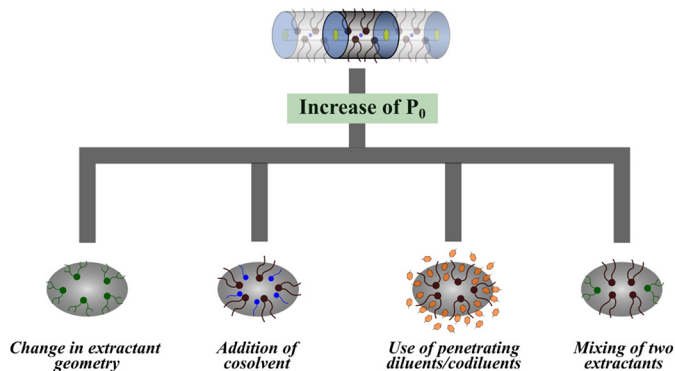
One can imagine the microstructure as a sponge formed by a living network that traps the diluent within its microstructure pores. If the network becomes too dense, the diluent is “squeezed out” and two macroscopic phases start to separate, but the phase transition is blocked due to high viscosity at the microphase separated state only. The presence of “nanocrystals” was already indicated experimentally. An increase at low  $q$  was observed in neutron scattering experiments indicating the presence of larger structures.

### 3.2.4 Application to the case of DEHIBA molecule

In contrast to an aqueous system containing an anionic surfactant and salt, where an asymptotic association-dissociation mechanism has to be considered [39], every uranyl ion in the organic phase can be seen as complexed. Therefore, it can be assumed that the area per extractant  $a_0$  at the polar/apolar interface increases linearly with complexed ions in the organic phase.

In order to demonstrate the effect of solvent penetration, the simulated curve was fitted to the experimental values by adjusting the variation of the area of head-group  $a_0$  with increasing uranyl concentration. Best agreement with the experimental results was found for the curve of 1.5 M DEHiBA using  $P_{0,\text{init}} = 2.6$  at  $x = 0$  and  $P_0 = 2.0$  at  $x = 0.44$ . The bending modulus  $\kappa^*$  was set to  $1.5 \text{ kT}$  per chain, thus  $3 \text{ kT}$  per molecule. For this case the scaling factor of equation (16) is equal to 1. The experimental agreement is shown in Figure 17, left. In order to simulate the effect of solvent penetration an additional parameter was introduced that denotes the percentage of increase in apolar volume (and therefore in the corresponding spontaneous packing parameter) by solvent penetration.

As can be seen in Figure 17, right, already a solvent penetration of 0.03 reduces the simulated viscosity significantly. That is in agreement with the findings in the experimental part that have shown that the penetrat-



**Fig. 18.** The four possibilities to tackle the problem of viscosity increase. All formulation approaches are based on an increase in spontaneous packing.

ing diluent xylene decreases the extent of viscosity increase and the COSMO-RS calculations of the  $\log_{10}(P_i^{E,D})$  values as well as the calculation of the activity coefficient calculation of an extractant in a given diluent.

## 4 Conclusion

This minimal model presented here and supported by experimental observations as well as COSMO-RS calculations allows propositions to optimize formulations of extracting solvents respective to viscosity. In order to reduce the viscosity once loaded in the presence of uranyle, the spontaneous packing parameter of the aggregating extractant molecules has to be increased as much as possible. Using this model presented here should also allow a reduction of the trial and error method used by parallel synthesis of dozen of extractants, in search for “the best”. Increased curvature leads to a higher concentration of endcap units, shortening the aggregate size and facilitating the shearing of the solution.

Regarding extractant solutions, a higher spontaneous packing parameter can be obtained by several formulation approaches (cf. Fig. 18). One possibility is to use extractants with a strongly curved structure, such as TBP or MOEHA. The latter molecule has a small complexing group and possesses two disymmetric chains, i.e. use of two different apolar chains. It was demonstrated for gemini extractants that decreasing the symmetry by two different chains results in larger spontaneous curvature allowing to assess stronger curved microphases [78].

A further promising approach is to use additives with a cosolvent effect. The addition of a cosolvent such as lipotropes [79] – short- and long chain alcohols or bulky hydrotropes – can also have a positive effect on the size of the headgroup and the apolar part. Addition of octanol is already a common tool in formulation of extractant solutions to prevent third phase formation [67,77].

Further, as was shown in this work, also the diluent itself has an influence on the spontaneous packing parameter and can therefore have a positive impact to the viscosity. Further, it was shown by Prabhu and co-workers, that the diluents can have also a huge impact on



distribution coefficients of different metals [11]. As an indicator for the propensity of a diluent to interact with extractant molecules and hence for the penetration power of a diluent into the protruding extractant chains, COSMO-RS predicted infinite dilution partition coefficients can be used, as it was demonstrated in this work.

And finally, as engineers have found by systematic essays that mixing two extractant molecules in a so-called “synergy formulation” [80] can have a positive effect on the viscosity. The addition can have two effects. First, the addition of a stronger curved extractant changes the mean curvature. Moreover, the addition of a second extractant can lead to a positive configurational entropic contribution that lowers the energy to form endcaps [81,82]. It can also be assumed that the stronger curved extractant accumulates at the more curved regions and stabilizes endcaps.

We thank Gilles Bordier, former Director in charge of technology of recycling, for getting our attention on the important technical problem that occurs in a large number of hydro-metallurgical processes, well beyond the nuclear fuel cycle that has been taken as an example. We further thank Matthias Pleines for fruitful discussions and help with the realization of the Monte-Carlo-like simulations on a hexagonal grid. M. Hahn thankfully acknowledges the financial and scientific support of Werner Kunz, Institute of Physical and Theoretical Chemistry, University of Regensburg. Thomas Zemb thanks Yves Bréchet, the High-commissar of the CEA for attributing to this work in 2014 the very first “thèse phare amont-aval” that associates crucial technical locks in practice to a fundamental “ieanic” approach considering energetic and structural aspects of species transferred between coexisting fluids.

## Author contribution statement

Maximilien Pleines was Ph.D. student at Marcoule Institute for Separation Chemistry and he wrote this article. His thesis entitles Viscosity control and prediction of microemulsions. Maximilian Hahn, Ph.D. student at the University of Regensburg, performed the COSMO-RS calculations of the extractants. Jean Duhamet and Thomas Zemb have contributed to this work by providing support and expert viewpoints.

## Supplementary Material

Extractant structures and COSMO cavities  
 Estimation of the spontaneous packing parameter from geometry  
 Hexagon definition for the Monte-Carlo-like Simulation

The Supplementary Material is available at <https://www.epj-n.org/10.1051/epjn/2019055/olm>.

## References

1. J. Rydberg, *Solvent extraction principles and practice*, 2nd edn. (M. Dekker, New York, 2004)

2. M.J. Hudson, An introduction to some aspects of solvent extraction chemistry in hydrometallurgy, *Hydrometallurgy* **9**, 149 (1982)
3. J.-F. Parisot, *Treatment and recycling of spent nuclear fuel: Actinide partitioning : application to waste management* (CEA, Paris, 2008)
4. T. Zemb, C. Bauer, P. Bauduin, L. Belloni, C. Déjournat, O. Diat, V. Dubois, J.-F. Dufrêche, S. Dourdain, M. Duvail, C. Larpent, F. Testard, P.S. Rostaing, Recycling metals by controlled transfer of ionic species between complex fluids: En route to “ieanics”, *Colloid Polym. Sci.* **293**, 1 (2015)
5. K. Osseo-Asare, Aggregation, reversed micelles, and microemulsions in liquid-liquid extraction: the tri-n-butyl phosphatediluent-water-electrolyte system, *Adv. Colloid Interface Sci.* **37**, 123 (1991)
6. F. Rodrigues, G. Ferru, L. Berthon, N. Boubals, P. Guilbaud, C. Sorel, O. Diat, P. Bauduin, J.P. Simonin, J.P. Morel, M.-N. Desrosiers, M.C. Charbonnel, New insights into the extraction of uranium(VI) by an N,N-dialkylamide, *Mol. Phys.* **112**, 1362 (2014)
7. P. Guilbaud, T. Zemb, Depletion of water-in-oil aggregates from poor solvents: Transition from weak aggregates towards reverse micelles, *Curr. Opin. Colloid Interface Sci.* **20**, 71 (2015)
8. N. Descouls, J.C. Morisseau, C. Musikas, 2015 Process for the extraction of uranium (VI) and/or plutonium (IV) present in an aqueous solution by means of N,N-dialkylamides. US Patent 4,772,429
9. T.H. Siddall, Effects of structure of N,N-disubstituted amides on their extraction of actinide and zirconium nitrates and of nitric acid, *J. Phys. Chem.* **64**, 1863 (1960)
10. P.N. Pathak, N,N-Dialkyl amides as extractants for spent fuel reprocessing: an overview, *J. Radioanal. Nucl. Chem.* **300**, 7 (2014)
11. D.R. Prabhu, A. Sengupta, M.S. Murali, P.N. Pathak, Role of diluents in the comparative extraction of Th(IV), U(VI) and other relevant metal ions by DHOA and TBP from nitric acid media and simulated wastes: Reprocessing of U–Th based fuel in perspective, *Hydrometallurgy* **158**, 132 (2015)
12. P.N. Pathak, A.S. Kanekar, D.R. Prabhu, V.K. Manchanda, Comparison of Hydrometallurgical Parameters of N,N-Dialkylamides and of Tri-n-Butylphosphate, *Sol. Extraction Ion Exch.* **27**, 683 (2009)
13. S. Abbott, *Surfactant Science*, [https://www.stevenabbott.co.uk/\\_downloads/Surfactant Science Principles and Practice.pdf](https://www.stevenabbott.co.uk/_downloads/Surfactant%20Science%20Principles%20and%20Practice.pdf)
14. H.J. Karam, J.C. Bellinger, Deformation and breakup of liquid droplets in a simple shear field, *Ind. Eng. Chem. Fundamentals* **7**, 576 (1968)
15. Q. Yang, H. Xing, B. Su, K. Yu, Z. Bao, Y. Yang, Q. Ren, Improved separation efficiency using ionic liquid–cosolvent mixtures as the extractant in liquid–liquid extraction: A multiple adjustment and synergistic effect, *Chem. Eng. J.* **181**, 334 (2012)
16. P. Ning, X. Lin, X. Wang, H. Cao, High-efficient extraction of vanadium and its application in the utilization of the chromium-bearing vanadium slag, *Chem. Eng. J.* **301**, 132 (2016)
17. P.N. Pathak, L.B. Kumbhare, V.K. Manchanda, Structural effects in N,N-Dialkyl amides on their extraction behavior towards uranium and thorium, *Sol. Extraction Ion Exch.* **19**, 105 (2001)

18. N. Condamines, P. Turq, C. Musikas, The extraction by N,N-dialkylamides III. A Thermodynamical approach of the multicomponent extraction organic media by a statistical mechanic theory, *Sol. Extr. Ion Exch.* **11**, 187 (1993)
19. K.K. Gupta, V.K. Manchanda, S. Sriram, G. Thomas, P.G. Kulkarni, R.K. Singh, Third phase formation in the extraction of uranyl nitrate by N,N-dialkyl aliphatic amides, *Sol. Extr. Ion Exch.* **18**, 421 (2000)
20. P.K. Verma, P.N. Pathak, N. Kumari, B. Sadhu, M. Sundararajan, V.K. Aswal, P.K. Mohapatra, Effect of successive alkylation of N,N-dialkyl amides on the complexation behavior of uranium and thorium: solvent extraction, small angle neutron scattering, and computational studies, *J. Phys. Chem. B* **118**, 14388 (2000)
21. E. Acher, Y. Hacene Cherkaski, T. Dumas, C. Tamain, D. Guillaumont, N. Boubals, G. Javierre, C. Hennig, P.L. Solari, M.-C. Charbonnel, Structures of plutonium(IV) and uranium(VI) with N,N-dialkyl amides from crystallography, X-ray absorption spectra, and theoretical calculations, *Inorg. Chem.* **55**, 5558 (2016)
22. G. Ferru, D. Gomes Rodrigues, L. Berthon, O. Diat, P. Bauduin, P. Guilbaud, Elucidation of the structure of organic solutions in solvent extraction by combining molecular dynamics and X-ray scattering, *Angew. Chem. Int. Ed* **53**, 5346 (2014)
23. G. Ferru, L. Berthon, C. Sorel, O. Diat, P. Bauduin, J.-P. Simonin, Influence of extracted solute on the organization of a monoamide organic solution, *Proc. Chem.* **7**, 27 (2012)
24. G.E.P. Box, J.S. Hunter, W.G. Hunter, *Statistics for experimenters: Design, innovation, and discovery*, 2nd edn. (Wiley-Interscience, Hoboken, NJ, 2005)
25. W. Davies, U. Gray, A rapid and specific titrimetric method for the precise determination of uranium using iron (II) sulphate as reductant, *Talanta* **11**, 1203 (1964)
26. A.R. Eberle, M.W. Lerner, C.G. Goldbeck, C.J. Rodden, Titrimetric determination of uranium in product, fuel and scrap materials after ferrous ion reduction in phosphoric acid; manual and automatic titration, in *Safeguards Techniques* (1970)
27. A. Klamt, Conductor-like screening model for real solvents: A new approach to the quantitative calculation of solvation phenomena, *J. Phys. Chem.* **99**, 2224 (1995)
28. A. Klamt, V. Jonas, T. Bürger, J.C.W. Lohrenz, Refinement and parametrization of COSMO-RS, *J. Phys. Chem. A* **102**, 5074 (1998)
29. A. Klamt, *COSMO-RS: From quantum chemistry to fluid phase thermodynamics and drug design*, 1st edn. (Elsevier, Amsterdam, 2005)
30. A.D. Becke, Density-functional exchange-energy approximation with correct asymptotic behavior, *Phys. Rev. A* **38**, 3098 (1988)
31. J.P. Perdew, Density-functional approximation for the correlation energy of the inhomogeneous electron gas, *Phys. Rev. B* **33**, 8822 (1986)
32. A. Klamt, G. Schüürmann, COSMO: A new approach to dielectric screening in solvents with explicit expressions for the screening energy and its gradient, *J. Chem. Soc., Perkin Trans. 2*, 799 (1993)
33. A. Schäfer, A. Klamt, D. Sattel, J.C.W. Lohrenz, F. Eckert, COSMO implementation in TURBOMOLE: extension of an efficient quantum chemical code towards liquid systems, *Phys. Chem. Chem. Phys.* **2**, 2187 (2000)
34. TURBOMOLE V7.2., University of Karlsruhe and Forschungszentrum Karlsruhe GmbH (1989–2007), TURBOMOLE GmbH (since 2007), 2017
35. F. Furche, R. Ahlrichs, C. Hättig, W. Klopper, M. Sierka, F. Weigend, Turbomole, *WIREs Comput. Mol. Sci.* **4**, 91 (2014)
36. A. Klamt, Conductor-like screening model for real solvents: a new approach to the quantitative calculation of solvation phenomena, *J. Phys. Chem. Hunter*, **99**, 2224 (1995)
37. A. Klamt, V. Jonas, T. Bürger, J.C.W. Lohrenz, Refinement and parametrization of COSMO-RS, *J. Phys. Chem. A* **102**, 5074 (1998)
38. A. Klamt, The COSMO and COSMO-RS solvation models, *WIREs Comput. Mol. Sci.* **8**, e1338 (2018)
39. M. Pleines, W. Kunz, T. Zemb, D. Benczédi, W. Fieber, Prediction of the viscosity peak of giant micelles in the presence of salt and fragrances, 2018, submitted
40. K. Shinoda, E. Hutchinson, Pseudo-phase separation model for thermodynamic calculations on micellar solutions, *J. Phys. Chem.* **66**, 577 (1962)
41. C. Tanford, The hydrophobic effect and the organization of living matter, *Science* **200**, 1012 (1978)
42. D.J. Mitchell, B.W. Ninham, Micelles, vesicles and microemulsions, *J. Chem. Soc. Faraday Trans. 2*, **77**, 601 (1981)
43. S.T. Hyde, I.S. Barnes, B.W. Ninham, Curvature energy of surfactant interfaces confined to the plaquettes of a cubic lattice, *Langmuir* **6**, 1055 (1990)
44. A. Fogden, S.T. Hyde, G. Lundberg, Bending energy of surfactant films, *Faraday Trans.* **87**, 949 (1991)
45. J.N. Israelachvili, D.J. Mitchell, B.W. Ninham, Theory of self-assembly of hydrocarbon amphiphiles into micelles and bilayers, *J. Chem. Soc., Faraday Trans. 2* **72**, 1525 (1976)
46. M.E. Cates, Reptation of living polymers: dynamics of entangled polymers in the presence of reversible chain-scission reactions, *Macromolecules* **20**, 2289 (1987)
47. M.E. Cates, S.J. Candau, Statics and dynamics of worm-like surfactant micelles, *J. Phys.: Condens. Matter* **2**, 6869 (1990)
48. M.E. Cates, S.M. Fielding, Rheology of giant micelles, *Adv. Phys.* **55**, 799 (2006)
49. F. Lequeux, Reptation of connected wormlike micelles, *Europhys. Lett.* **19**, 675 (1992)
50. S.J. Candau, A. Khatory, F. Lequeux, F. Kern, Rheological behaviour of wormlike micelles: Effect of salt content, *J. Phys. IV France* **03**, C1-197 (1993)
51. A. Khatory, F. Lequeux, F. Kern, S.J. Candau, Linear and nonlinear viscoelasticity of semidilute solutions of wormlike micelles at high salt content, *Langmuir* **9**, 1456 (1993)
52. S. May, Molecular packing in cylindrical micelles, in *Giant micelles: properties and applications*, edited by R. Zana (Taylor & Francis, Boca Raton, 2007), pp. 41–80
53. C.R. Safinya, E.B. Sirota, D. Roux, G.S. Smith, Universality in interacting membranes: The effect of cosurfactants on the interfacial rigidity, *Phys. Rev. Lett.* **62**, 1134 (1989)
54. P. Pieruschka, S. Marčelja, Statistical mechanics of random bicontinuous phases, *J. Phys. II France* **2**, 235 (1992)
55. N. Condamines, C. Musikas, The extraction by N,N-Dialkylamides. II. Extraction of actinide cations, *Sol. Extr. Ion Exch.* **10**, 69 (1992)
56. G. Ferru, Spéciation moléculaire et supramoléculaire des systèmes extractants à base de monoamides, Dissertation, 2013
57. B. Moeser, D. Horinek, The role of the concentration scale in the definition of transfer free energies, *Biophys. Chem.* **196**, 68 (2015)

58. B.K. Paul, S.P. Moulik, The viscosity behaviours of microemulsions: An overview, *Proc. Indian Natl. Sci. Acad. Pt. A* **66**, 499 (2000)
59. M. Pleines, Viscosity-control and prediction of microemulsions, Dissertation, University of Montpellier/Regensburg, 2018
60. T. Tlustý, Defect-induced phase separation in dipolar fluids, *Science* **290**, 1328 (2000)
61. A.G. Zilman, S.A. Safran, Role of cross-links in bundle formation, phase separation and gelation of long filaments, *Europhys. Lett.* **63**, 139 (2003)
62. B. Bharti, A.-L. Fameau, M. Rubinstein, O.D. Velev, Nanocapillarity-mediated magnetic assembly of nanoparticles into ultraflexible filaments and reconfigurable networks, *Nat. Mater.* **14**, 1104 (2015)
63. E.N. da C. Andrade, LVIII., A theory of the viscosity of liquids – Part II, *Lond. Edinb. Dublin Philos. Mag. J. Sci.* **17**, 698 (2009)
64. N. Ouerfelli, Z. Barhoumi, O. Iulian, Viscosity Arrhenius activation energy and derived partial molar properties in 1, 4-dioxane + water binary mixtures from 293.15 to 323.15 K, *J. Sol. Chem.* **41**, 458 (2012)
65. S.G.E. Giap, The hidden property of Arrhenius-type relationship: Viscosity as a function of temperature, *J. Phys. Sci* **21**, 29 (2010)
66. L. Berthon, L. Martinet, F. Testard, C. Madic, T. Zemb, Solvent penetration and sterical stabilization of reverse aggregates based on the DIAMEX process extracting molecules: consequences for the third phase formation, *Sol. Extr. Ion Exch.* **25**, 545 (2007)
67. B. Abécassis, F. Testard, T. Zemb, L. Berthon, C. Madic, Effect of n-octanol on the structure at the supramolecular scale of concentrated dimethyldioctylhexylethoxymalonamide extractant solutions, *Langmuir* **19**, 6638 (2003)
68. N.P. Franks, M.H. Abraham, W.R. Lieb, Molecular organization of liquid n-octanol: an X-ray diffraction analysis, *J. Pharma. Sci.* **82**, 466 (1993)
69. Y. Marcus, Structural aspects of water in 1-octanol, *J. Sol. Chem.* **19**, 507 (1990)
70. A.S.C. Lawrence, M.P. McDonald, J.V. Stevens, Molecular association in liquid alcohol-water systems, *Trans. Faraday Soc.* **65**, 3231 (1969)
71. P. Bauduin, F. Testard, L. Berthon, T. Zemb, Relation between the hydrophile/hydrophobe ratio of malonamide extractants and the stability of the organic phase: investigation at high extractant concentrations, *Phys. Chem. Chem. Phys.* **9**, 3776 (2007)
72. T.N. Zemb, The DOC model of microemulsions: Microstructure, scattering, conductivity and phase limits imposed by sterical constraints, *Colloids Surf. A* **129**, 435 (1997)
73. P.A. Forsyth, S. Marčelja, D.J. Mitchell, B.W. Ninham, Onsager transition in hard plate fluid, *J. Chem. Soc., Faraday Trans. 2* **73**, 84 (1977)
74. D. Avnir, The fractal approach to heterogeneous chemistry: Surfaces, colloids, polymers (John Wiley & Sons, Chichester, 1992)
75. A. Parker, W. Fieber, Viscoelasticity of anionic wormlike micelles: Effects of ionic strength and small hydrophobic molecules, *Soft Matter* **9**, 1203 (2013)
76. V.A. Parsegian, *Van der Waals forces: A handbook for biologists, chemists, engineers, and physicists* (Cambridge University Press, Cambridge, 2006)
77. F. Testard, T. Zemb, P. Bauduin, L. Berthon, Third-phase formation in liquid-liquid extraction: a colloidal approach, *ChemInform* **41**, i (2010)
78. R. Oda, S.J. Candau, I. Huc, Gemini surfactants, the effect of hydrophobic chain length and dissymmetry, *Chem. Commun.* **21**, 2105 (1997)
79. P. Bauduin, F. Testard, T. Zemb, Solubilization in alkanes by alcohols as reverse hydrotropes or “lipotropes”, *J. Phys. Chem. B* **112**, 12354 (2008)
80. S.K. Singh, P.S. Dhama, S.C. Tripathi, A. Dakshinamoorthy, Studies on the recovery of uranium from phosphoric acid medium using synergistic mixture of (2-Ethyl hexyl) Phosphonic acid, mono (2-ethyl hexyl) ester (PC88A) and Tri-n-butyl phosphate (TBP), *Hydrometallurgy* **95**, 170 (2009)
81. J. Rey, Étude des mécanismes d'extraction synergiques en séparation liquide-liquide. Dissertation, University of Montpellier, 2016
82. J. Rey, S. Dourdain, L. Berthon, J. Jestin, S. Pellet-Rostaing, T. Zemb, Synergy in extraction system chemistry: combining configurational entropy, film bending, and perturbation of complexation, *Langmuir* **31**, 7006 (2015)

**Cite this article as:** Maximilian Pleines, Maximilian Hahn, Jean Duhamet, Thomas Zemb, A minimal predictive model for better formulations of solvent phases with low viscosity, *EPJ Nuclear Sci. Technol.* **6**, 3 (2020)